Book Chapter

Signal Transmission Analysis in Implantable Human Body Communication for Abdominal Medical Devices

Dairoku Muramatsu* and Miyu Kodama

The University of Electro-Communications, Japan

***Corresponding Author:** Dairoku Muramatsu, The University of Electro-Communications, 1-5-1 Chofugaoka, Chofu, Tokyo 182-8585, Japan

Published **April 26, 2024**

This Book Chapter is an excerpt of an article published by Dairoku Muramatsu and Miyu Kodama at AIP Advances in August 2023. (Dairoku Muramatsu, Miyu Kodama. Signal transmission analysis in implantable human body communication for abdominal medical devices. AIP Advances 13, 085022 (2023); doi: 10.1063/5.0157485)

How to cite this book chapter: Dairoku Muramatsu, Miyu Kodama. Signal transmission analysis in implantable human body communication for abdominal medical devices. In: Prime Archives in Sensors: 3rd Edition. Hyderabad, India: Vide Leaf. 2024.

Acknowledgments: A part of this research was funded by JSPS KAKENHI, Takahashi Industrial and Economic Research Foundation, KDDI Foundation, and Murata Science and Education Foundation.

Conflict of Interest: The authors have no conflicts to disclose.

Author Contributions: Dairoku Muramatsu: Conceptualization (lead); Data curation (equal); Formal analysis (lead); Funding acquisition (lead); Investigation (lead); Methodology (equal); Project administration (lead); Resources (lead); Software (lead); Supervision (lead); Validation (lead); Visualization (lead); Writing – original draft (lead); Writing – review & editing (lead). **Miyu Kodama**: Conceptualization (supporting); Data curation (equal); Formal analysis (supporting); Investigation (supporting); Methodology (equal); Validation (supporting); Visualization (supporting); Writing – original draft (supporting); Writing – review & editing (supporting).

Data Availability: The data supporting the findings of this study are available from the corresponding author upon reasonable request.

Abstract

Implantable medical devices, such as neurostimulators, need to be wirelessly controlled from outside the body. Many of these devices use high-frequency signals in the 400 MHz, 900 MHz, and 2.45 GHz bands to communicate with external devices. However, high-frequency bands can suffer from signal attenuation in biological tissues and from electromagnetic interference with surrounding devices. In contrast, human body communication (HBC) uses relatively low frequencies in the 3–30 MHz band, which can alleviate signal attenuation and prevent emissions outside the body during communication. In this study, we investigated the use of HBC for implantable medical devices in the abdomen using electromagnetic field

simulations. The results showed that the transmission between the transmitter inside the body and the receiver outside the body was adequate for stable communication. However, when the receiver was detached from the skin surface, the transmission characteristics rapidly decreased. Moreover, when the receiver and skin were separated by 1 mm, the transmission degraded by 34 dB, indicating that electromagnetic interference between the implanted transmitter and surrounding devices (including other medical devices) is rare. Finally, we evaluated the proposed system from the perspective of medical electromagnetic compatibility and human safety. The simulation results demonstrated that the radiated emissions and human exposure of the HBC system meet international standards.

Introduction

Chronic pain affects 1.5×10^9 people worldwide [1,2]. Spinal cord stimulation (SCS) is a treatment that alleviates pain by applying electrical stimulation to the spinal cord [3,4]. To perform SCS, a stimulator is implanted in the lower abdomen, and it must be wirelessly controlled from outside the body, as shown in Figure 1(a). Many implantable medical devices use high-frequency signals in the 400 MHz, 900 MHz, and 2.45 GHz bands to communicate with external devices [5–8]. However, these high-frequency bands suffer from signal attenuation in biological tissues [9–14] and from electromagnetic interference with other electrical devices [15–20]. Table I lists the wireless medical devices and home appliances that can potentially interfere with implantable medical devices. Clearly, unconventional wireless communication technologies that do not use airborne electromagnetic waves are needed. Human body communication (HBC) is a wireless communication technology that uses the human body as a transmission path for electrical signals [21,22]. In HBC, electrical signals are

transmitted through electrodes that are placed on the human body. HBC enables low-power, low-noise, and secure communications because the electric field is distributed only in the vicinity of the human body. Unlike conventional far-field antenna systems, HBC generally uses a quasistatic near-field [23] excited at relatively low frequencies in the 3–30 MHz band, considerably lower than the resonant frequency of HBC electrodes. Accordingly, HBC can alleviate signal attenuation and prevent emissions outside the body during communication [24]. Although studies have been conducted on HBC with mobile and wearable devices, such as smartphones and smartwatches [25–28], HBC for implantable medical devices has not been sufficiently studied [29,30].

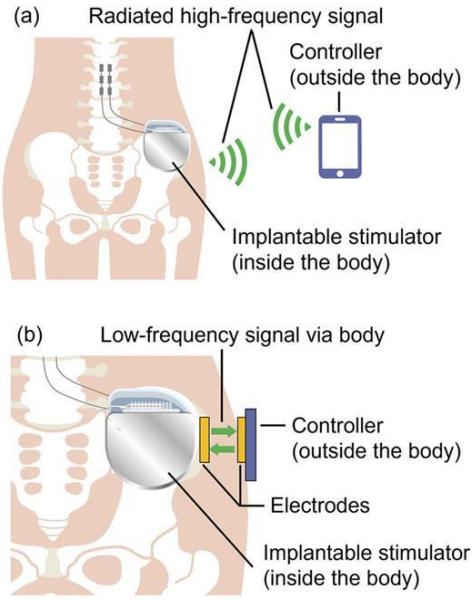

Figure 1: (a) Conventional wireless communication system for an implantable stimulator. (b) Proposed human body communication system for an implantable stimulator.

Table I: Wireless medical devices and home appliances that can interfere with implantable medical devices.

Standard	Frequency	Device example
…	20–100 kHz	Induction cooker
Industrial, scientific, and medical (ISM) 13.56 MHz band	13.56 MHz	RFID and wireless charging devices
Medical Device Radiocommunications Service (MedRadio)	401–457 MHz	Medical telemetry systems, pacemakers, capsule endoscopy systems, and defibrillators
ISM 2.45 GHz band	2.4–2.5 GHz	Microwave ovens, Bluetooth, insulin pumps, and neurostimulators
IEEE 802.11n	2.4–2.5 GHz	WiFi devices
	5.15–5.35 GHz	
	5.47–5.725 GHz	

In this study, we propose and investigate the use of HBC for medical devices that are implanted in the abdomen, as shown in Figure 1(b). We aim to clarify the mechanism for signal propagation in and around the body and analyze the basic communication characteristics, such as transmission characteristics and electric field distributions.

Simulation Setup

An electromagnetic field simulation model, shown in Figure 2, was used to study the communication between an implantable abdominal medical device and a controller on the skin surface. The dimensions of the abdominal model were determined based on the average shape of a Japanese adult male [31]. The model was composed of skin, fat, and muscle layers, and we determined the electrical properties of each tissue layer referencing our previously developed electromagnetic phantoms, which can be used at 10–30 MHz [32], Table II lists the relative permittivity and conductivity of each layer. Using the electrical properties of phantoms will facilitate a comparison between future simulations and experimental

results. The overall dimensions of the abdominal model were 260 × 210 × 190 mm^3, and the thicknesses of the skin, fat, and muscle layers were 2, 6, and 182 mm, respectively. To determine the thickness of each tissue layer, we considered the thickness range of each abdominal tissue [33]. The thickness ranges reasonably compared with those in conventional studies of multi-layer abdominal tissue phantoms [34,35]. The implantable device (sized 48 × 48 × 10 mm^3) was fixed to the fascia within 2 cm of the skin surface, reproducing the situation of actual implantable stimulators [36]. A free space was created in the muscle layer to accommodate the device housing [36]. In this study, the implantable device was the transmitter (TX) and the controller outside the body was the receiver (RX). An 8 × 24 mm^2 two-electrode structure, commonly used in wearable HBC systems [27,37], was used as the communication electrode, which was placed in the center of the model. The TX electrode was placed in contact with the lower part of the fat layer, while the RX electrode was placed on the surface of the skin layer. From a human safety perspective, implantable electrodes should be formed from biocompatible materials, such as titanium [36]. We confirmed that the electrical conductivity of titanium (0.6–2.0 × 10^6 S/m) electrodes does not affect signal transmission in terms of an electrode material. Therefore, all electrodes were constructed from perfect electrical conductors. The impedance of the TX electrode at the feeding point and the receiving load of the RX were both 50 Ω. When selecting the signal frequency (10 MHz), we consulted previous studies [38,39] and considered the 13.56-MHz industry–science–medical band [40]. The finite-difference time-domain method-based electromagnetic field simulator XFdtd (Remcom Inc., PA, USA) was used to calculate the transmission characteristics, electric field distributions, and input impedance of the electrodes. The computing space of the simulation was represented by non-uniform grids, with grid

sizes of 1 mm around the electrodes and 2 mm at the edge of the computing space. The distance between the model edge and the absorbing boundary was 20 cells thick. The absorbing boundary was a perfectly matched layer composed of seven sublayers. The time step of the calculation was 1.926 ps.

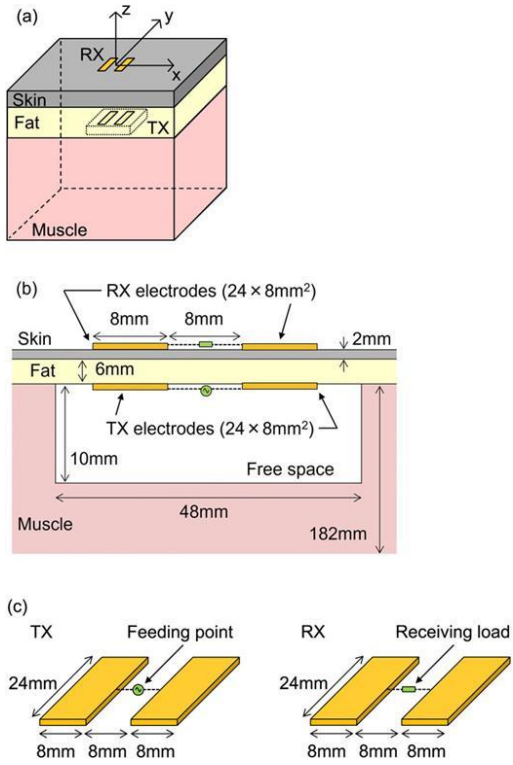

Figure 2: (a) Overview of the simulation model. (b) Side view of the simulation model in cross section including the feed point. (c) Transmitter (TX) and receiver (RX) models.

Table II: Electrical properties of the abdominal model.[**32]**

Layer	Relative permittivity ε_r	Conductivity σ (S/m)
Skin	421	0.17
Fat	71	0.028
Muscle	184	0.67

Results and Discussion

A. Transmission Characteristics and Electric Field Distributions

In this study, we used the transmission characteristic $|S_{21}|$ to express the ratio between the received power at the RX and the available power at the TX. The simulation results revealed that $|S_{21}|$ was −22 dB, which is sufficient for stable communication. This is because the TX and RX electrodes are positioned in close proximity to each other through the skin and fat layers. To investigate the signal propagation mechanism in greater detail, we calculated the electric field distribution around and inside the model, as shown in Figure 3. The observational plane includes the feeding point of the TX and the receiving load of the RX. The electric field distribution demonstrated that the TX and RX electrodes are strongly coupled across the skin and fat layers. The signal from the TX propagates strongly toward the skin layer where the RX is located, whereas only a weak signal propagates toward the deeper muscle layer. The propagation strengths differ because the free space inside the implantable device insulates the TX electrodes and the muscle layer. Signal transmission in HBC is contributed by conductive currents through biological tissues. In the direction of the muscle layer, signal propagation is heavily attenuated by the insulation of free space, preventing unwanted signal propagation.

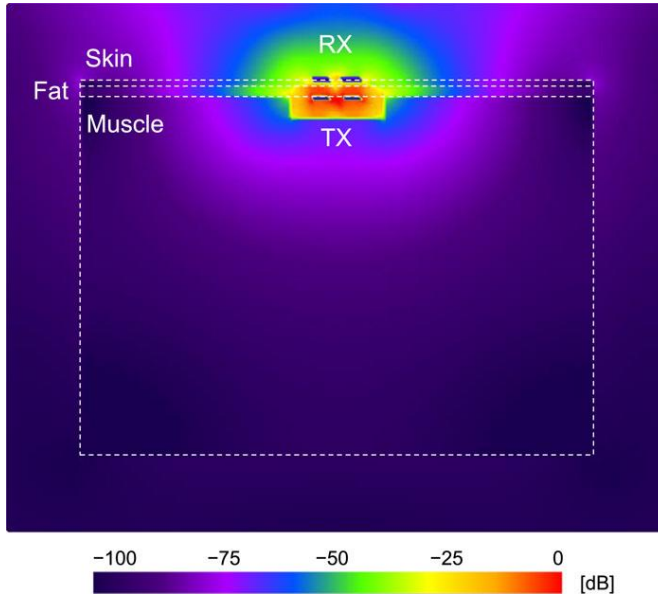

Figure 3: Electric field distribution in cross section, including the feed point.

The ultimate sensitivity of the commonly used Bluetooth module is approximately −70 to −80 dBm. For example, the SH-M08 Bluetooth module used in the wireless neurostimulator system has an ultimate sensitivity of −84 dBm [41]. When $|S_{21}|$ is −22 dB in the configuration of this study, the feeding point requires 20 nW (−48 dBm) input power to satisfy the ultimate sensitivity of −70 dBm. This implies that implantable HBC can reduce power consumption compared to conventional wireless communication methods.

Moreover, we calculated the input impedance of the TX electrode to be $Z_{in} = 299 - j412\ \Omega$, which deviates considerably from the 50 Ω output impedance at the feeding point. This is because the electrode structure was intended to be worn on the wrist. To resolve this impedance mismatch at the feeding point and to effectively input more

of the signal into the body, the electrode structure must be optimized for implantable usage.

B. Influence of Displacement between Devices

To investigate the impact of the displacement between devices inside and outside the body, we calculated $|S_{21}|$ by shifting the RX position horizontally and vertically. Figure 4 displays the RX's horizontal (x–y) and vertical (z–x) displacements. In the horizontal plane, we displaced the RX by 24 and 48 mm in the x and y directions from the center of the abdomen model, respectively. In the vertical plane, we displaced the RX up to 10 mm in 1 mm increments while maintaining the center in the horizontal plane.

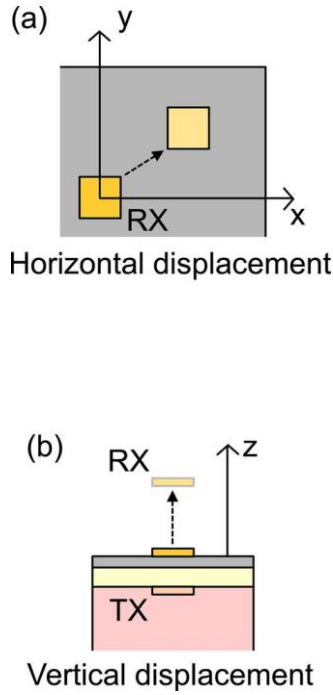

Figure 4: (a) Displacement of the receiver in the horizontal plane (x–y). (b) Displacement of the receiver in the vertical plane (z–x).

As shown in Figure 5, $|S_{21}|$ decreased as we displaced the RX from the center of the abdominal model, directly above the TX. This is because the electric field generated by the TX became weak as the RX moved further from the center of the TX position, as shown in Figure 3. To prevent unintended signal interruption due to device displacement, it is desirable to fix both devices with magnets via the body during communication, as in transcutaneous optical couplers [42]. To clarify the maximum allowable displacement, we calculated the displacement ranges that fulfill the ultimate sensitivity (−70 dBm) of the RX when the TX outputs 0.01 mW (−20 dBm), the power output of Bluetooth Low Energy Power Class 3 at an approximate communication distance of 1 m [43]. A sufficient power in both the *x* and *y* directions was received at horizontal displacements within 24 mm. Therefore, the maximum achievable distance in both *x* and *y* directions was estimated as 24 mm.

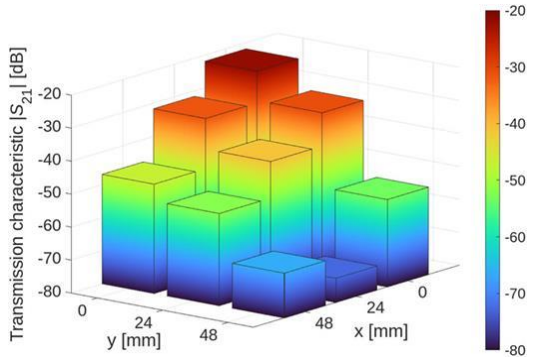

Figure 5: Transmission characteristics as a function of the horizontal position of the receiver.

When the distance between the RX electrodes and the skin surface *z* was 1 mm, $|S_{21}|$ was approximately −56 dB, as shown in Figure 6. This value is 34 dB smaller than that calculated when *z* was 0 mm, i.e., the RX electrodes were firmly attached to the skin. As the RX moved further away from the skin surface, $|S_{21}|$ decreased at an approximate rate

of 1.6 dB/mm. This implies that signal transmission will be lost when the RX is removed from the body. This decrease in $|S_{21}|$ is also illustrated by the electric field distribution shown in Figure 3. These results indicate that the signal from the implanted TX rarely causes electromagnetic interference with surrounding devices, such as other medical devices, because the signal attenuates rapidly as the RX moves away from the body surface. In addition, based on the duality of antennas, implanted HBC devices are considered robust against electromagnetic interference from surrounding devices.

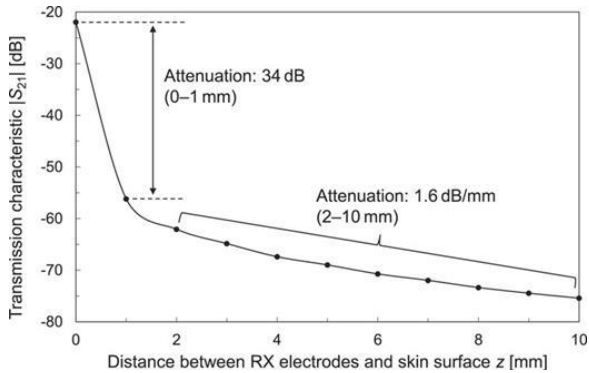

Figure 6: Transmission characteristics as a function of the vertical position of the receiver.

C. Medical Electromagnetic Compatibility and Human Safety Evaluation

We also evaluated the proposed system from the perspective of medical electromagnetic compatibility (EMC). The radiated emission limit for medical devices [group 1, class B] is 40 dB μV/m at a distance of 3 m from the device [44]. In the proposed system, the electric field strength at 30 cm from the TX was ~17 dB μV/m when the TX inputted 1 μW power to meet the ultimate sensitivity of the RX. This means that the radiated emission from the proposed system is clearly below the limit level. Therefore, implantable HBC can achieve superior medical EMC

compared to conventional wireless communication methods.

To assess the human safety of the proposed system, we adopted the specific absorption rate (SAR), which determines human exposure to an electromagnetic field. The SAR (in W/kg) defines the power of a radio frequency electromagnetic field absorbed by 1 kg of human tissue. It is calculated as SAR = $\sigma E2/\rho$, where E is the RMS electric field within the tissue, σ is the electrical conductivity of the tissue sample, and ρ is the sample density. As the averaging scheme of SAR, we selected 1 g averaging. Under the same conditions as medical EMC evaluation, the peak SAR per 1 g of abdominal tissue in direct contact with the electrodes was 1.6×10^{-4} W/kg, sufficiently smaller than the regional absorption limit (1.6 W/kg per 1 g of any tissue) in the safety guidelines [45,46]. Therefore, the proposed system meets the human safety criterion within a sufficient margin.

D. Electromagnetic Phantoms and Flexible Electrodes

This study mainly focused on the analytical aspects of implantable HBC. For future experimental studies, we developed electromagnetic phantoms and flexible HBC electrodes. Figure 7 depicts the cross-sectional view of the abdominal phantoms comprising the skin, fat, and muscle layers. The TX electrodes were embedded inside the muscle layer, and the RX electrodes were affixed to the skin layer. "The overall dimensions of the phantom were 100 mm on each side, and the thicknesses of the skin, fat, and muscle layers were 2, 6, and 92 mm, respectively. Considering the electrical properties of each biological tissue, the phantom was constructed with conductive silicone for the skin layer, soybean oil and 12-hydroxystearic acid for the fat layer, and deionized water, sodium chloride, and agar for the muscle layer. Figure 8 illustrates the flexible HBC electrodes made of rolled copper and gold plating on a polyimide substrate, identical to the two-electrode structure used in the analysis of this study. The flexible HBC electrodes can be either embedded in the phantom or adhered to its surface. By utilizing these

experimental tools, we aim to investigate the signal propagation mechanisms of implantable HBC in future research.

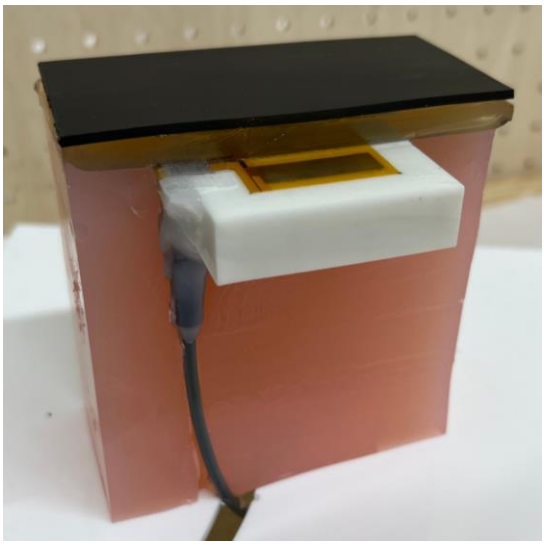

Figure 7: Cross-sectional view of abdominal phantoms comprising skin, fat, and muscle layers.

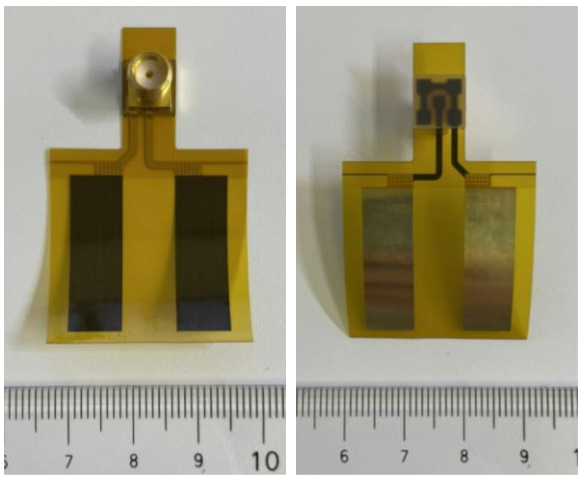

Figure 8: Flexible HBC electrodes made of thin copper and gold plating on a polyimide substrate.

Conclusion

We investigated the use of implantable HBC for medical devices implanted in the abdomen using electromagnetic field simulations. The results showed that the transmission characteristic $|S_{21}|$ between the transmitter (TX) and receiver (RX) was −22 dB, which is sufficient for stable communication. To understand the signal propagation mechanism of HBC, we examined the electric field distribution around and inside the abdominal model. We also investigated the influence of displacement between the devices inside and outside the body by calculating $|S_{21}|$ when shifting the RX position. The horizontal displacement of the RX had a considerable effect on $|S_{21}|$, suggesting that the position of the devices should be fixed during communication. When the RX was moved away from the skin surface, $|S_{21}|$ rapidly decreased due to the signal propagation mechanism of HBC, which uses the body as a transmission path for signals. We also evaluated the proposed system from the perspective of medical electromagnetic compatibility and human safety. The results showed that the radiated emission and human exposure of the proposed HBC system was adequately small according to the limitation in international standards. These results can be used not only for the development of implantable HBC for abdominal medical devices but also for general implantable applications. HBC signals can also power implantable devices deep inside the body [47]. In future work, we will investigate appropriate electrode structures and signal frequencies of implantable HBC devices through experiments on both electromagnetic phantoms and test animals.

References

1. EB Stevens, GJ Stephens. Recent advances in targeting ion channels to treat chronic pain: Editorial, Br. J. Pharmacol. 2018; 175: 2133–2137.
2. RD Treede, W Rief, A Barke, Q Aziz, MI Bennett, et al. Chronic pain as a symptom or a disease: The IASP classification of chronic pain for the international classification of diseases (ICD-11), Pain. 2019; 160: 19–27.
3. J Caylor, R Reddy, S Yin, C Cui, M Huang, et al. Spinal cord stimulation in chronic pain: Evidence and theory for mechanisms of action, Bioelectron. Med. 2019; 5: 12.
4. EA Joosten, G Franken. Spinal cord stimulation in chronic neuropathic pain: Mechanisms of action, new locations, new paradigms, Pain. 2020; 161: S104–S113.
5. Medtronic BV. PillCamTM Capsule Endoscopy User Manual. 2016.
6. MK Aktas, W Zareba, J Butler, A Younis, S McNitt, et al. Confirm Rx insertable cardiac monitor for primary atrial fibrillation detection in high-risk heart failure patients (Confirm-AF trial). Ann. Noninvasive Electrocardiol. 2023; 28: e13021.
7. Iqbal, M Al-Hasan, IB Mabrouk, TA Denidni. Wireless powering and telemetry of deep-body ingestible bioelectronic capsule, IEEE Trans. Antennas Propag. 2022; 70: 9819–9830.
8. OF Celik, SC Ba saran. Compact triple-band implantable antenna for multitasking medical devices, J. Electr. Eng. 2022; 73: 166–173.
9. MA Jensen, Y Rahmat-Samii. EM interaction of handset antennas and a human in personal communications, Proc. IEEE. 1995; 83: 7–17.
10. Y Chan, MQH Meng, KL Wu, X Wang. In IEEE Engineering in Medicine and Biology 27th Annual Conference. IEEE. 2005; 7754–7757.
11. Alomainy, Y Hao. Modeling and characterization of biotelemetric radio channel from ingested implants considering organ contents. IEEE Trans. Antennas Propag. 2009; 57: 999–1005.
12. Mauludiyanto, G Hendrantoro, MF Nova. The attenuation

characteristics of the body tissue on frequency function in WBAN channel, JAREE. 2021; 5: 107–113.
13. S Benaissa, L Verloock, D Nikolayev, M Deruyck, G Vermeeren, et al. Propagation-loss characterization for livestock implantables at (433, 868, 1400) MHz, IEEE Trans. Antennas Propag. 2021; 69: 5166–5170.
14. MJ Christoe, J Yuan, A Michael, K Kalantar-Zadeh. Bluetooth signal attenuation analysis in human body tissue analogues. IEEE Access. 2021; 9: 85144–85150.
15. American national standard recommended practice for an on-site, ad hoc test method for estimating electromagnetic immunity of medical devices to radiated radio-frequency (RF) emissions from RF transmitters, ANSI C63.18-2014, Revision of ANSI C63.18-1997). 2014; 1–64.
16. V Buzduga, D Witters, J Casamento, W Kainz. Testing the immunity of active implantable medical devices to CW magnetic fields up to 1 MHz by an immersion method. IEEE Trans. Biomed. Eng. 2007; 54: 1679–1686.
17. T Toyoshima. In 2011 IEEE MTT-S International Microwave Workshop Series on Innovative Wireless Power Transmission: Technologies, Systems, and Applications. IEEE. 2011; 101–104.
18. MS Darweesh, T Ismail, H Mostafa. In 2018 11th International Symposium on Communication Systems, Networks and Digital Signal Processing (CSNDSP). 2018; 1–6.
19. YC Yalcin, C Kooij, DAMJ Theuns, AA Constantinescu, JJ Brugts, et al. Emerging electromagnetic interferences between implantable cardioverter-defibrillators and left ventricular assist devices. EP Eur. 2020; 22: 584–587.
20. T Nishikawa, T Hikage, M Yamamoto. In 2022 IEEE International Workshop on Electromagnetics: Applications and Student Innovation Competition (IWEM). IEEE. 2022; 124–125.
21. TG Zimmerman. Personal area networks: Near-field intrabody communication. IBM Syst. J. 1996; 35: 609–617.
22. D Naranjo-Hernandez, A Callejon-Leblic, ˇZL Vasi´c, M Seyedi, YM Gao. Past results, present trends, and future challenges in intrabody communication. Wireless Commun. Mob. Comput. 2018; 9026847.

23. D Das, S Maity, B Chatterjee, S Sen. Enabling covert body area network using electro-quasistatic human body communication. Sci. Rep. 2019; 9: 4160.
24. J Wang. Wide band human body communication technology for wearable and implantable robot control. IEICE Trans. Commun. E103. 2020; 6: 628–636.
25. K Zhao, Z Ying, S He. Intrabody communications between mobile device and wearable device at 26 MHz. IEEE Antennas Wirel. Propag. Lett. 2017; 16: 1875–1878.
26. J Jeong, K Park, C Lee. Design of cavity-backed bow-tie antenna with matching layer for human body application. Sensors. 2019; 19: 4015.
27. D Muramatsu, K Sasaki. Transmission analysis in human body communication for head-mounted wearable devices. Electronics. 2021; 10: 1213.
28. Q Huang, W Alkhayer, ME Fouda, A Celik, AM Eltawil. In 2022 IEEE-EMBS International Conference on Wearable and Implantable Body Sensor Networks (BSN). IEEE. 2022; 1–5.
29. MN Islam, MR Yuce. Review of medical implant communication system (MICS) band and network, ICT Express. 2016; 2: 188–194.
30. Han, J Mao, X Wang, S Yu, Z Zhang. In 2021 IEEE International Symposium on Circuits and Systems (ISCAS). IEEE. 2021; 1–5.
31. K Makiko, M Masaaki. Japanese 3-D body shape and dimensions data 2003, H18PRO-503. National Institute of Advanced Industrial Science and Technology. 2006.
32. Muramatsu, F Koshiji, K Koshiji, K Sasaki. Multilayered phantom for input impedance evaluation of human body communication electrodes. EAI Endorsed Trans. Cogn. Commun. 2015; 2: 313.
33. WFW Southwood. The thickness of the skin. Plast. Reconstr. Surg. 1955; 15: 423–429.
34. Q Bonds, T Weller. In IEEE International Conference on Microwaves, Antennas, Communications and Electronic Systems (COMCAS). IEEE. 2017; 1–4.
35. HM Bernety, RD Puckett D. Schurig, and C. Furse, Comparison of passive 2-D and 3-D ring arrays for medical telemetry focusing, IEEE Antennas Wireless Propag. Lett.

2019; 18: 1189–1193.
36. St. Jude Medical. Proclaim implantable pulse generator clinician's manual. 2017.
37. K Fujii, M Takahashi, K Ito. Electric field distributions of wearable devices using the human body as a transmission channel. IEEE Trans. Antennas Propag. 2007; 55: 2080–2087.
38. Muramatsu, F Koshiji, K Koshiji, K Sasaki. Analytical and experimental studies on human body communication between wristwatch and handheld devices using muscle homogenous phantom at 10 MHz. Sens. Mater. 2014; 26: 581–589.
39. Y Nishida, K Sasaki, K Yamamoto, D Muramatsu, F Koshiji. Equivalent circuit model viewed from receiver side in human body communication. IEEE Trans. Biomed. Circuits Syst. 2019; 13: 746–755.
40. Radio regulations, edition of 2020: Vol. 1: Articles. International Telecommunication Union. 2020.
41. Ersoz, H Phu, I Kim, M Han. In 2019 41st Annual International Conference of the IEEE Engineering in Medicine and Biology Society (EMBC). IEEE. 2019; 5200–5203.
42. Tanigawa, K Shiba, K Koshiji, K Tsuchimoto, K Tsukahara, et al. Transcutaneous optical telemetry system for a totally implantable artificial heart investigation of transcutaneous optical coupler consisting of three light emitting and receiving devices. Artificial Organs. 2000; 29: 315–321.
43. Bluetooth core specification 5.3. Core Specification Working Group. 2021.
44. CISPR 11, IEC. Geveva, Switzerland. 2019.
45. RF Cleveland, JL Ulcek. Questions and answers about biological effects and potential hazards of radiofrequency electromagnetic fields Federal Communications Commission, Washington, DC, USA. 1999.
46. IEEE standard for safety levels with respect to human exposure to radio frequency electromagnetic fields, 3 kHz to 300 GHz (IEEE C95.1-2005. IEEE. 2006.
47. Y Ma, Z Luo, C Steiger, G Traverso, F Adib. In Proceedings of the 2018 Conference of the ACM Special Interest Group on Data Communication. ACM, Budapest Hungary, 2018;

417–431.